# Journal of Materials Chemistry B

Accepted Manuscript






ROYAL SOCIETY OF CHEMISTRY

www.rsc.org/materialsB

Journal of Materials Chemistry B RSCPublishing

ARTICLE

# Pickering high internal phase emulsion-based hydroxyapatite/poly(ε-caprolactone) nanocomposite scaffolds

Cite this: DOI: 10.1039/xoxxoooooox

Received ooth January 2012,
Accepted ooth January 2012

DOI: 10.1039/xoxxoooooox

www.rsc.org/

Yang Hu,[a] Huichang Gao,[b] Zhengshan Du,[a] Yixiao Liu,[a] Yu Yang[a] and Chaoyang Wang*[a]

Biocompatible, biodegradable and bioactive nanocomposite (NC) scaffolds with well-defined interconnected porous structures have attracted increasing attention in bone tissue engineering. In this work, we develop a facile method to fabricate poly(L-lactic acid)-modified hydroxyapatite (g-HAp)/poly(ε-caprolactone) (PCL) NC porous scaffolds by solvent evaporation based on water-in-dichloromethane (W/O) Pickering high internal phase emulsion (HIPE) templates, which are stabilized with g-HAp nanoparticles. The resultant porous scaffolds demonstrate interconnected and rough pore structures, which can be adjusted readily by varying g-HAp nanoparticle concentration, PCL concentration and the internal phase volume fraction. Moreover, the investigation of mechanical property and in vitro biomineralization activity exhibit that the Young's modulus, compressive stress and bioactivity of the fabricated porous scaffolds are significantly enhanced with increasing the g-HAp nanoparticle concentration. In addition, in vitro drug release studies of the porous scaffolds using ibuprofen (IBU) as a model drug show that the loaded IBU displays a sustained release profile. In vitro cell culture assays confirm that mouse bone mesenchymal stem cells can adhere, spread, and proliferate on the porous scaffolds, indicating that the porous scaffolds are biocompatible. All these results suggest that the fabricated g-HAp/PCL NC scaffolds have a promising potential for bone tissue engineering application.

## Introduction

Bone tissue engineering has been considered as an emerging and promising approach to repair damaged or diseased bones.[1-4] In this regard, one of the important issues is the development of appropriate three-dimensional bio-scaffolds as bone graft substitutes.[5,6] These scaffolds should not only mimic the architecture and physiological functions of the native bone extracellular matrices (ECM) for cell adhesion, proliferation, migration and differentiation, but also be able to act as temporary functional template for the new bone formation.[7-9] To achieve these goals, the ideal scaffolds designed for the bone tissue engineering applications should meet certain specific requirements, including excellent biocompatibility, good bioactivity, highly interconnected porosity to promote cell seeding and nutrient diffusion, controllable biodegradability at a commensurate rate with bone remodelling, and proper mechanical strength to endure the environment stress.[10-13] Furthermore, it should be noted that the implantation of scaffolds is likely to cause local inflammation response. Fortunately, the incorporation of anti-inflammatory drug into scaffolds is capable of effectively attenuating the local inflammation response.[14] Therefore, the scaffolds should also have the drug loading and controlled release properties to arrive the long-term anti-inflammatory effect.

Natural bone is an innate hybrid biomaterial composed of organic and inorganic constituents,[15] which are mainly represented by type I collagen and hydroxyapatite (HAp) crystals, respectively.[16,17] Inspired by the compositions of natural bone, many studies have applied biodegradable polymers and bioactive ceramics to fabricate bone engineering scaffolds.[18-22] Among various biopolymer materials, synthetic biodegradable polyesters have been extensively investigated in recent years. In particular, poly(ε-caprolactone) (PCL) has attracted great attention because of its excellent biocompatibility, mechanical strength, processability and adjustable biodegradability.[23-25] On the other hand, synthetic calcium phosphate bioceramics, especially nano-HAp, have been broadly studied and recognized as very promising inorganic biomaterials for the development of nanocomposite (NC) scaffolds for bone tissue engineering applications.

Synthetic nano-HAp not only has a chemical similarity to the inorganic component of nature bone, but also exhibits outstanding bioactivity, biocompatibility, mechanical property, absorbability and osteoconductivity.[26-28] Recently, HAp/PCL NC scaffolds were reported to have excellent cell viability, bioactivity, mechanical property and controllable biodegradability.[16,22,29] Therefore, highly porous HAp/PCL NC scaffolds have been regarded as potential candidates for bone repair and regeneration. However, the lack of interface adhesion between PCL matrix and nano-HAp filler leads to early failure at the PCL-HAp interface,[5,30] because non-polar PCL and natural HAp are thermodynamically immiscible. In this regard, surface modification of HAp nanoparticles is a promising approach to improve the interface adhesion strength between PCL matrix and HAp nanoparticles.[31] In term of the bone tissue engineering application, HAp nanoparticles should be surface-modified using biodegradable and biocompatible materials, such as PLLA, PLGA and PCL. Wang et al. reported that PCL-modified HAp/PCL porous scaffolds were fabricated by thermally induced phase separation/salt leaching technique, and these scaffolds demonstrated improved mechanical properties compared to the relevant HAp/PCL porous scaffolds.[30] Nonetheless, the above literature involved a complex and time-consuming procedure for the removal of porogens. Thus, it is highly desirable to develop a facile and effective approach to fabricate surface-modified HAp/PCL NC porous scaffolds.

To date, several approaches have been developed to fabricate NC porous scaffolds composed of polymers and inorganic nanoparticles, including particulate leaching,[32] freeze drying,[33] electrospinning,[34] and Pickering high internal phase emulsion (HIPE) templating.[35-37] Among these approaches, Pickering HIPE templating has obtained increasing attention due to its simple protocols, low cost and wide choice of materials. Pickering HIPE is defined as a colloid particle-stabilized emulsion with the internal phase volume fraction larger than 74%.[38-42] After solidifying the emulsion external phase, the emulsion droplets can act as templates for pores and once the solvent removal from emulsion results in a macroporous NC scaffolds.[43-45] In Pickering HIPE droplets, colloid particles are nearly irreversible adsorption at the oil-water interface, which makes the resulted emulsions very stable.[46-51] Thus, Pickering HIPE droplets are very effective templates for the formation of NC porous scaffolds with defined porous structures. Despite obvious progress has been made in the preparation of NC porous materials from Pickering HIPEs, the production of surface-modified HAp/PCL porous scaffolds by Pickering HIPE templates has not been reported. Herein, we reported the facile preparation of PLLA-modified HAp (g-HAp)/PCL NC porous scaffolds by solvent evaporation from templating Pickering HIPEs. To be specific, dichloromethane ($CH_2Cl_2$) dispersion (oil phase) containing g-HAp nanoparticles and PCL was homogenized with water (aqueous phase) to form water-in-dichloromethane (W/O) Pickering HIPEs. Then, porous scaffolds were readily obtained by solvent evaporation from the prepared HIPEs. The influences of g-HAp nanoparticle concentration, PCL concentration and internal phase volume fraction on the pore structures of porous scaffolds were investigated. Next, the mechanical property, biomineralization activity, anti-inflammatory drug (ibuprofen, IBU) release profile and biocompatibility of the porous scaffolds were further evaluated.

## Experimental

### Materials

PCL (average molecular weight MW=80 000 g/mol) was purchased from Sigma-Aldrich. $CH_2Cl_2$ was supplied by Guangzhou Chemical Factory (Guangzhou, China). The preparation of HAp and g-HAp nanoparticles have been described in our previous study.[52] The mean diameter of g-HAp nanoparticles measured by dynamic light scattering was about 580 nm. The amount of grafted PLLA on g-HAp nanoparticles determined using thermal gravimetric analysis was about 5.5 wt%. IBU was provided by Dalian Melone Pharmaceutical Co., Ltd. (Dalian, China). Mouse bone mesenchymal stem cells (BMSCs) were bought from the American Type Culture Collection (ATCC, Manassas, VA). Dulbecco's modified eagle medium (DMEM) and fetal bovine serum (FBS) were obtained from Gibco (Carlsbad, CA, USA). All materials were used as received without purification. Water used in this study was produced by deionization and filtration using a Millipore purification apparatus (resistivity larger than 18.0 MΩ cm).

### Fabrication of g-HAp/PCL porous scaffolds

The g-HAp/PCL porous scaffolds were fabricated using solvent evaporation of W/O Pickering HIPEs. The typical preparation procedure was described as follows. PCL was completely dissolved in $CH_2Cl_2$ with mechanical shaking. Then the g-HAp nanoparticles were added to the as-prepared $CH_2Cl_2$ solution of PCL. The solution mixture was treated by ultrasound at 0 $^oC$ for 30 min to obtain a good dispersion of g-HAp nanoparticles. Afterwards, water was added to the above dispersion in batches and then hand-shaking at every turn to form Pickering HIPE. The total emulsion volume was maintained at 10 mL. Furthermore, the Pickering HIPE was then dried at room temperature in a fume hood to remove $CH_2Cl_2$ and water. Herein, the resultant porous scaffolds were coded as $H_xP_y$-*z*, which indicated that the relevant Pickering HIPE was prepared with the g-HAp nanoparticle concentration of *x* w/v% with respect to oil phase, PCL concentration of *y* w/v% with respect to oil phase and the internal phase volume fraction (the ratio of the aqueous phase volume to the total emulsion volume) of *z* v/v%.

### Characterization of Pickering HIPEs and g-HAp/PCL porous scaffolds

The Pickering HIPEs were placed on microscope slides and observed using a microscope (Carl Zeiss, German) equipped with a COOLPIX 4500 digital camera (Nikon, Japan).

The interior morphologies of the porous scaffolds were studied with a Zeiss EVO 18 field emission scanning electron microscope (SEM) fitted with an X-ray energy dispersive spectrometer (EDS). Before observation, the scaffolds were sectioned with a sharp razor



 

blade after being frozen in liquid nitrogen. And the scaffold samples were sputtered with gold to avoid sample-charging effects and observed with an accelerating voltage of 10 kV.

Fourier transform infrared spectroscopy (FTIR) of the scaffold samples were measured using a German Vector-33 IR instrument in the 4000 - 500 $cm^{-1}$ spectral range. Before measurement, the scaffold samples were ground with KBr power and then pressed into pellets.

The porosity (*P*) of the porous scaffold was determined by the following procedure. Firstly, the volumes and mass of the porous scaffold and the relevant non-porous film were measured respectively. Then the apparent density of porous scaffold ($\rho_S$) and the bulk densityof non-porous film ($\rho_f$) were gained by calculating the mass/volume ratio of the relevant samples. Finally, the porosity of the scaffold sample was calculated using the following equation:

$$P\ (\%) = (1 - \rho_S/\rho_f) \times 100 \qquad (1)$$

Three measurements for each scaffold were carried out and the mean value of porosity was taken.

The mechanical properties of the porous scaffolds were assessed by compression tests. The scaffold samples were about 11 mm in diameter and 8 mm in height. The tests were performed using a SLBL-1KN material testing machine (Shimadzu, Japan) at room temperature under a load of 500 N. The stress-strain curves of the scaffold samples were recorded at a cross-head displacement speed of 1.0 mm/min. The compressive modulus was performed from the elastic region of the stress-strain curve. Three identical specimens for each scaffold sample were tested and the results were the mean values.

The in vitro biomineralization of the porous scaffolds were investigated in 1.5 times simulated body fluid (1.5SBF). The scaffold sample with a diameter of about 11 mm and thickness of 4 mm was weighed ($W_0$) and immersed in 30 mL 1.5SBF solution at 37 $^oC$. Three identical specimens for every scaffold sample were used for each experiment. The 1.5SBF solution was refreshed every other day to ensure enough ionic concentrations for mineral nucleation and growth. After incubation for 4, 7, 14, 21 and 28 days, the scaffold samples were removed and rinsed with water three times, and subsequently air-dried at room temperature. Furthermore, the resultant scaffold sample was measured ($W_t$). The weight increase of scaffold sample (*W*) after incubation in 1.5SBF was calculated by the following equation:

$$W\ (\%) = [(W_t - W_0)/W_0] \times 100 \qquad (2)$$

**Drug loading and in vitro release of g-HAp/PCL porous scaffolds**

The drug-loaded porous scaffolds were prepared according to the preparation procedure of porous scaffolds as mentioned above except $CH_2Cl_2$ dispersion containing IBU (5.0 wt%, with respect to the total weight of g-HAp and PCL). The loading efficiency of IBU in porous scaffolds was determined by the solvent extraction method as described in our previous report.[14] Briefly, the IBU-loaded porous scaffold was weighted and soaked in ethanol. Then the samples in triplicate were incubated for 24 h at 150 rpm. After centrifugation at 5 000 rpm for 5 min, the supernatant was analysed using an UV-Vis spectrophotometer at 222 nm. The amount of loaded drug was calculated using the standard curve established from standard ethanol solutions of IBU. And the loading efficiency (LE) of drug was obtained according to the following equation:

$$LE\ (\%) = (M_t/M_0) \times 100 \qquad (3)$$

where $M_t$ and $M_0$ represent the mass of loaded drug and total added drug, respectively.

The drug release from porous scaffolds was measured by putting 30 mg of IBU-loaded scaffolds into different glass vials containing 30 mL of phosphate buffer saline (PBS, pH 7.4). For comparison, the release of free IBU was also determined by placing IBU into a dialysis bag (cut-off MW 8000 g/mol) with 5 mL of PBS, and then immersing the dialysis bag in a glass vial containing 25 mL of PBS. All the glass vials were incubated at 37 $^oC$ with shaking at 100 rpm. At each pre-determined time interval, 2 mL of release solution was removed and then measured using an UV-Vis spectrophotometer at 222 nm. After each sampling, 2 mL of fresh PBS was added to maintain constant volume. The accumulated drug release was calculated according to the calibration curve of the drug in PBS solution. Each experiment was performed in triplicate, and the average value was reported.

**In vitro biocompatibility assay**

BMSCs were used to evaluate the biocompatibility of the porous scaffolds. BMSCs were cultured in DMEM supplemented with 10% (v/v) FBS at 37 $^oC$ in a 5% $CO_2$ incubator. The culture medium was refreshed every 3 days. Once BMSCs had grown to confluence, they were removed using 0.25% trypsin-EDTA solution and resuspended in culture medium at a density of $5\times10^4$ cells/mL. Before cell culture, the porous scaffolds were sterilized with 75% ethanol and ultraviolet (UV) light at room temperature for 6 h, and then rinsed with sterile PBS solution three times. And the porous scaffolds were pre-wetted in culture medium overnight.

Cell viability was assessed by 3-(4,5-dimethylthiazol-2-yl)-2,5-diphenyl tetrazolium bromide (MTT) assay. Briefly, the porous scaffolds (6 mm in diameter and 2 mm in thickness) were fixed in 96-well tissue culture plates (TCPS). Then 40 μL of BMSCs suspension containing $2\times10^3$ cells was evenly seeded onto the pre-wetted scaffolds. The cell/scaffold constructs were incubated at 37 $^oC$ for 3 h in a 5% $CO_2$ incubator, and additional 160 μL of fresh culture medium was added to every well. The cell culture medium was renewed every other day. After incubation of 1, 4 and 7 days, the culture media were discarded and the cell/scaffold constructs were rinsed three times with PBS. 100 μL MTT solution (5 mg $mL^{-1}$) was added to each well and incubated for 4 h at 37 $^oC$. After removal of the upper medium, 150 μL of dimethyl sulfoxide was introduced to each well to dissolve the intracellular formazan crystals, and then 100 μL of the obtained solution was pipetted into 96-well TCPS. Furthermore, the absorbance value was detected at 570 nm using a spectrophotometric microplate reader. The cells cultured on bare TCPS were used as a negative control. Three specimens for every scaffold sample were tested, and the average value was reported.

The morphology of BMSCs was evaluated by SEM. The porous scaffolds with a diameter of about 11 mm and thickness of 2 mm were fixed in 24-well TCPS. 200 μL of BMSCs suspension containing $1\times10^4$ cells was seeded evenly onto the pre-wetted scaffolds. After incubation at 37 $^oC$ for 3 h in a 5% $CO_2$ incubator, 1

mL of fresh culture medium was added into each well. The culture medium was refreshed every two days. After 4 and 7 days of culture, the cell/scaffold constructs were washed twice with PBS, fixed in 2.5% glutaraldehyde solution for 4 h, and subsequently dehydrated using a graded ethanol series. After drying, the cell/scaffold samples were sputter-coated with gold and observed using SEM.

## Results and Discussion

### Fabrication of NC porous scaffolds

The g-HAp/PCL NC porous scaffolds with highly porous structures were simplely and effectively fabricated via W/O Pickering HIPE templates. Initially, water was added in batches into a $CH_2Cl_2$ dispersion containing g-HAp nanoparticles and PCL, and then the mixture was hand shaked to form g-HAp nanoparticle-stabilized Pickering HIPE. Herein, $CH_2Cl_2$ was chosen as solvent for oil phase, because it was fairly volatile and could be readily eliminated by evaporation even at room temperature. Furthermore, $CH_2Cl_2$ has been widely used to prepare NC porous bioscaffolds. The studied HIPE formulations are listed in **Table 1**. The stable HIPEs were formed for all formulations, and drop test indicated that all obtained HIPEs were W/O type emulsions. These HIPEs could be stored for 1 month without any phase separation. The typical optical microscope image of Pickering HIPE $H_5P_5$-80 (Fig. S1) showed that the emulsion droplets were packed and spherical, and their sizes were polydisperse. Serving as control experiments, the emulsification of $CH_2Cl_2$ and water, $CH_2Cl_2$ solution of PCL and water, $CH_2Cl_2$ dispersion of HAp nanoparticles and water, and $CH_2Cl_2$ dispersion of g-HAp nanoparticles and water were performed. The first three control systems failed to produce HIPEs, while the last control system succeeded in forming stable HIPEs. This result indicated that g-HAp nanoparticles were obviously necessary toward stable HIPEs. Therefore, it was confirmed that g-HAp nanoparticles were efficient particulate emulsifiers to prepare highly stable and concentrated W/O Pickering emulsions without any additional surfactants.

The NC porous scaffolds were easily fabricated by air drying of the prepared W/O Pickering HIPEs at room temperature. The digital photographs of typical sample $H_5P_5$-80 before and after air drying are shown in Fig. S2. It was observed that the bulk scaffold underwent significant shrinkage during drying. The shrinkage could be mainly ascribed to the removal of the liquid phase from precursor HIPE during drying process. Actaully, all bulk scaffolds had different degrees of shrinkage during drying from corresponding precursor HIPEs. The cross-sections of prepared NC porous scaffolds were characterized by SEM to observe the inner pore structures. The representative SEM images (**Fig. 1-3** and Fig. S3,4) exhibited that all scaffolds possessed an interconnected porous structure with the pore sizes ranging from several microns to over one hundred microns. In addition, the pore wall of porous scaffolds was rough due to g-HAp nanoparticles attached on or filled into the pore wall surfaces. Although the obvious shrinkage was presented in drying process, the macroporous scaffolds with interconnected and rough pore structure were indeed successfully fabricated. Therefore, it was concluded that the prepared Pickering HIPEs could be used as effective initial templates to form hierarchical g-HAp/PCL scaffolds. Herein, in order to prepare HIPE templated porous scaffolds with different pore structures, we exhibited three simple but effective ways to control the droplet structure morphology in emulsion templates and thus the pore structures of porous scaffolds; we tried to adjust g-HAp nanoparticle concentration, PCL concentration and internal phase volume fraction (IPVF).

**Table 1.** Processing parameters and physical properties of g-HAp/PCL NC scaffolds.

| Samples | g-HAp (w/v%) | PCL (w/v%) | IPVF (v/v%) | $\rho_f$ (g cm$^{-3}$) | $\rho_s$ (g cm$^{-3}$) | P (%) |
|---|---|---|---|---|---|---|
| $H_{2.5}P_5$-80 | 2.5 | 5 | 80 | 1.464 | 0.108 | 92.6 |
| $H_5P_5$-80 | 5 | 5 | 80 | 1.625 | 0.171 | 89.5 |
| $H_{7.5}P_5$-80 | 7.5 | 5 | 80 | 1.722 | 0.291 | 83.1 |
| $H_{10}P_5$-80 | 10 | 5 | 80 | 1.786 | 0.311 | 82.6 |
| $H_5P_{2.5}$-80 | 5 | 2.5 | 80 | 1.789 | 0.174 | 90.3 |
| $H_5P_{7.5}$-80 | 5 | 7.5 | 80 | 1.528 | 0.299 | 80.7 |
| $H_5P_{10}$-80 | 5 | 10 | 80 | 1.465 | 0.357 | 75.6 |
| $H_5P_5$-75 | 5 | 5 | 75 | 1.625 | 0.304 | 80.1 |
| $H_5P_5$-85 | 5 | 5 | 85 | 1.625 | 0.141 | 91.3 |
| $H_5P_5$-90 | 5 | 5 | 90 | 1.625 | 0.102 | 93.7 |

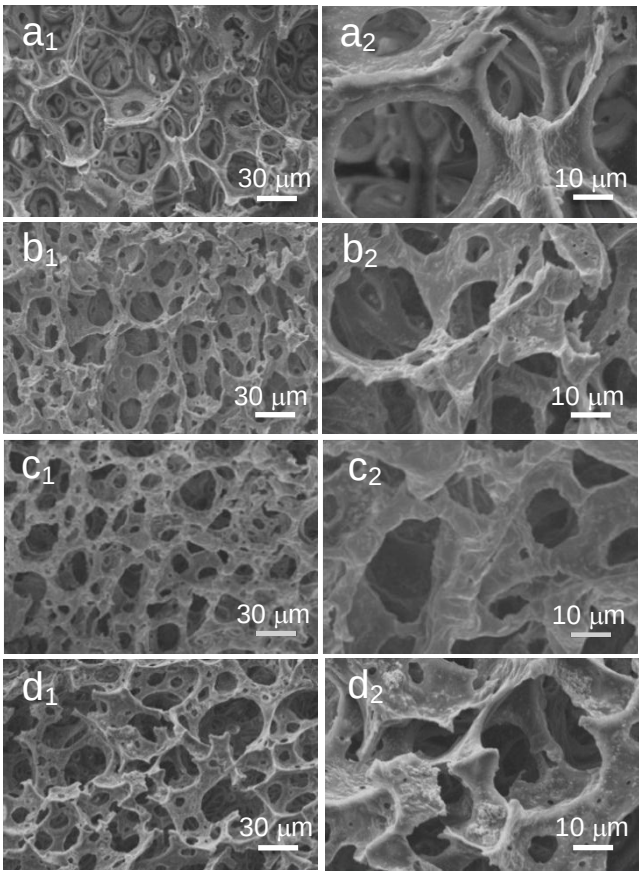


**Fig. 1** SEM micrographs of porous scaffolds prepared from Pickering HIPE ($a_1$, $a_2$) $H_{2.5}P_5$-80, ($b_1$, $b_2$) $H_5P_5$-80, ($c_1$, $c_2$) $H_{7.5}P_5$-80 and ($d_1$, $d_2$) $H_{10}P_5$-80 with g-HAp nanoparticle concentrations of 2.5, 5, 7.5 and 10 w/v%, respectively.

**Fig. 1** shows SEM micrographs of porous scaffolds prepared with different g-HAp concentrations. As observed, increasing g-HAp

nanoparticle concentration in the oil phase from 2.5 to 7.5 w/v% resulted in a gradual decrease in the pore sizes and pore throat sizes of the resultant porous scaffolds. This should be the reason that with the increase of g-HAp nanoparticle concentration in the oil phase, more nanoparticles were used to stabilize emulsions, which improved the stability of emulsions and formed smaller emulsion droplets, and thus reduced the pore size and pore throat size of the porous scaffolds. With further increase of g-HAp nanoparticle concentration (10 w/v%), the pore sizes and pore throat sizes of the porous scaffolds increased mildly on the contrary. This was because the excess g-HAp nanoparticles could aggregate at the W/O interface and in the oil phase, which decreased the stabilization of the emulsions and resulted in droplet coalescence to form larger droplets, and hence enhanced pore size and pore throat size. As expected, with the increase of g-HAp nanoparticle concentration, more g-HAp nanoparticles presented on pore wall surfaces and hence the roughness of pore wall surfaces enhanced. Furthermore, increasing the g-HAp nanoparticle concentration enhanced the density and decreased the porosity of the porous scaffolds (Table 1). This result should be the reason that with more g-HAp nanoparticles added in PCL matrix, the solid volume of the building materials enhanced while the pore sizes presented a decrease trend.

SEM micrographs of porous scaffolds prepared with varying PCL concentrations are presented in **Fig. 2** and Fig. S3. At low PCL concentration (2.5 w/v%), the fibrous pore walls were observed in the porous scaffold. Increasing the PCL concentration from 5 to 10 w/v% decreased the pore sizes and pore throat sizes of the porous scaffolds, and resulted in forming the more intact and thicker pore walls. This could be attributed to the reason that the higher PCL concentration assisted to form wider and thicker continuous phase films around the emulsion droplets, which increased the emulsion stability and the polymer film thickness between the neighboring droplets, thus decreased the pore sizes and pore throat sizes and increased the pore wall thickness. As the same reason, the density of the porous scaffolds enhanced, and the porosity decreased with the increase of PCL concentration (Table 1).

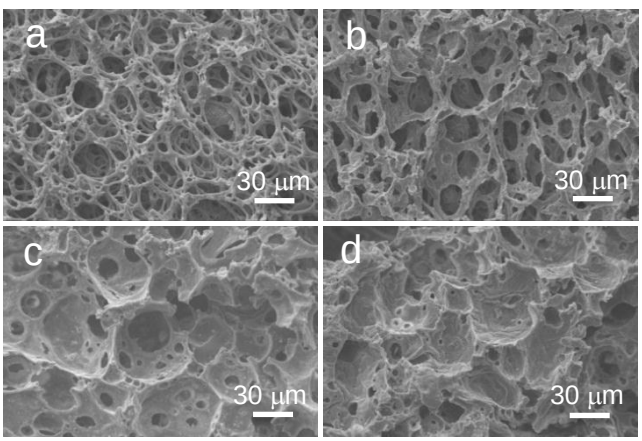


**Fig. 2** SEM micrographs of porous scaffolds prepared from Pickering HIPE (a) $H_5P_{2.5}$-80, (b) $H_5P_5$-80, (c) $H_5P_{7.5}$-80 and (d) $H_5P_{10}$-80 with the PCL concentrations of 2.5, 5, 7.5 and 10 w/v%, respectively.

**Fig. 3** and Fig. S4 display SEM micrographs of porous scaffolds prepared with different internal phase volume fractions. It was observed that increasing internal phase volume fraction enhanced the pore sizes and pore throat sizes of porous scaffolds. This should be assigned to the fact that with the increase of internal phase volume fraction, the larger w/o interface surface should be stabilized with nanoparticles, which resulted in the formation of sparsely packed particle layers at the w/o interface and the destabilization of HIPEs, and thus caused larger pore sizes and pore throat sizes of NC porous scaffolds. As expected, with increasing internal phase volume fraction, the density of porous scaffolds reduced and the porosity enhanced (Table 1). Based on above discussion, porous scaffolds with different pore structures can be readily fabricated by varying the g-HAp nanoparticle concentration, PCL concentration or internal phase volume fraction of the HIPE templates.

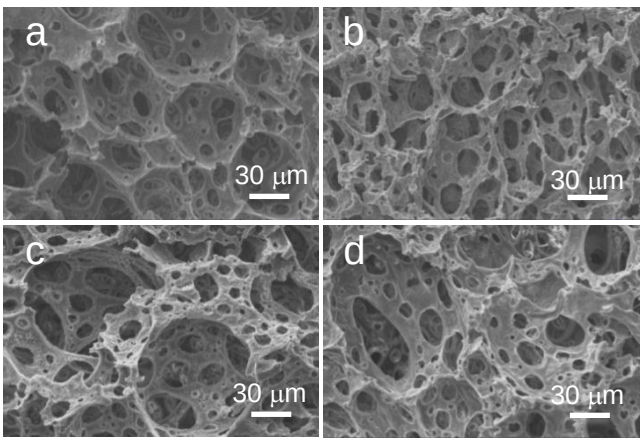


**Fig. 3** SEM micrographs of porous scaffolds prepared from Pickering HIPE (a) $H_5P_5$-75, (b) $H_5P_5$-80, (c) $H_5P_5$-85 and (d) $H_5P_5$-90 with the internal phase volume fractions of 75, 80, 85 and 90 v/v%, respectively.

**Mechanical property of NC porous scaffolds**

Scaffolds used for bone tissue engineering should have certain mechanical strength and stiffness to resist physiological loads during the bone regeneration process. Herein, the mechanical properties of porous scaffolds were evaluated by compression tests. The typical compressive stress-strain curves for porous scaffolds fabricated at varying g-HAp nanoparticle concentrations are presented in **Fig. 4**a. And the Young's modulus and compressive stress at 45% strain of various porous scaffolds are summarized in Fig. 4b. As observed, all porous scaffolds clearly showed similar typical stress-strain curves, which had three discrete regions with an initial elastic region, a collapse plateau region and a densification region. As the g-HAp concentration increased, both the Young's modulus and compressive stress at 45% strain of porous scaffolds obvously enhanced, which implied that g-HAp nanoparticles helped to enhance the rigidity of porous scaffolds. With the increase in g-HAp concentration, the improvement of Young's modulus and compressive stress could be attributed to the enhancement of stress transfer from the PCL matrix to the rigid g-HAp nanoparticles. Furthermore, increasing the g-HAp concentration enhanced the density and reduced the porosity of porous scaffolds, which should be another reason for the

improvement of Young's modulus and compressive stress. Thus, porous scaffolds with different mechanical properties could be readily fabricated varying the g-HAp nanoparticle concentration.

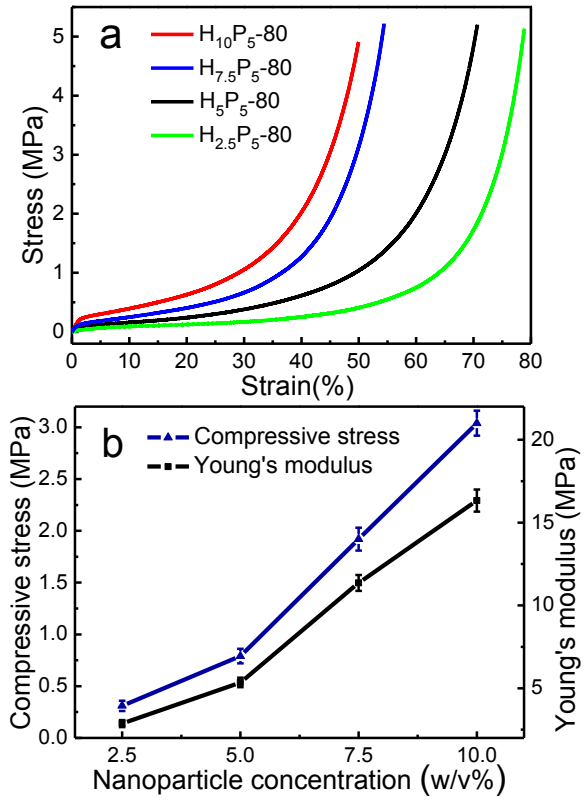


**Fig. 4** (a) Typical compressive stress–strain curves, (b) Young's modulus and compressive stress at 45% strain of porous scaffolds fabricated at varying g-HAp nanoparticle concentrations.

### In vitro biomineralization of NC porous scaffolds

Besides mechanical property, the bone-forming ability is another important indice in the fabrication of porous scaffolds for bone tissue engineering application. Thus, the in vitro biomineralization tests were conducted to testify the bone-forming ability of porous scaffolds. Herein, the porous scaffolds were incubated in 1.5SBF up to 28 days. The mass changes of porous scaffolds prepared at varying g-HAp nanoparticle concentrations versus the incubation time are presented in **Fig. 5**a. As observed, all porous scaffolds exhibited an obvious mass increase with increasing incubation time. The first mass increase of porous scaffolds was observed after 4-day mineralization (an early mineralization stage), indicating that initial deposition of apatite minerals appeared even at the early mineralization stage. This showed that the porous scaffolds had excellent apatite mineralization ability. In addition, it was also seen that the mass increase of porous scaffolds containing higher g-HAp nanoparticles was significantly faster for the same incubation time. The result suggested that higher g-HAp nanoparticle content added into PCL matrix promoted the deposition of apatite minerals on porous scaffolds. This could be ascribed to the exposure of g-HAp nanoparticles on the PCL matrix surface provided nucleation initiation sites for apatite mineral formation and growth.[52] Thus, increasing g-HAp nanoparticle content enhanced the nucleation initiation sites and consequently accelerated the formation and growth of apatites on the porous scaffolds. In short, the incorporation of g-HAp nanoparticles into PCL was an effective way to enhance the biomineralization activity of polymer scaffolds, which could enhance the osteoinductive properties of porous scaffolds.[3]

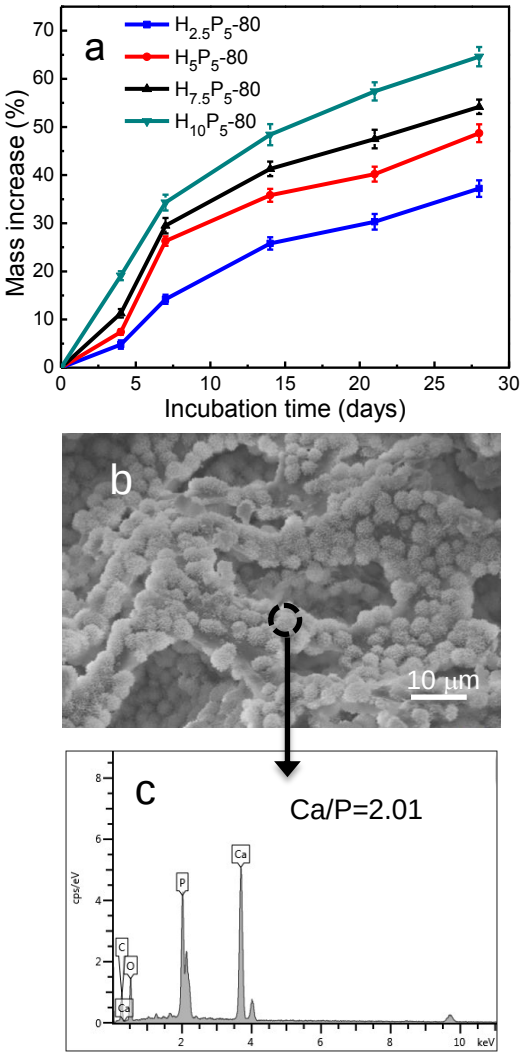


**Fig. 5** (a) Mass increase vs mineralization time in 1.5SBF for different porous scaffolds. (b) SEM image displaying morphology of the apatite particles formed on scaffold $H_{7.5}P_5$-80 incubated in 1.5SBF after 14 days. (c) EDS spectrum reveals the apatite composition on the circular area in (b).

To assess the morphology of the apatite minerals formed on the porous scaffolds, the mineralized porous scaffolds were characterized using SEM. A typical SEM image of scaffold $H_{7.5}P_5$-80 incubated in 1.5SBF after 14 days is shown in Fig. 5b. It was seen that the spherical apatite particles were deposited on the pore wall surface of mineralized porous scaffold, which resulted in the increase of pore wall roughness. And the sizes of apatite particles were mainly varying from 2 to 4 μm. During the SEM observation,

the composition of the apatite particles was also analyzed by EDS (Fig. 5c). The EDS spectra showed that apatite particles were mainly composed of carbon (C), oxygen (O), phosphorus (P) and calcium (Ca). Furthermore, it was also found that the atomic molar ratio of calcium to phosphorus (Ca/P) of apatite was 2.01, which was higher than that of the pure HAp (1.67), implying that the mineral particles deposited on porous scaffolds were "calcium-sufficient apatite". It might be ascribed to the partial substitution of $CO_3^{2-}$ groups for $PO_4^{3-}$ groups in the incubation process.

**In vitro release kinetics**

To investigate drug release from the NC porous scaffolds, we have employed a widely used anti-inflammatory drug (IBU) as the model drug. Herein, IBU was added into $CH_2Cl_2$ dispersion to prepare drug-loaded porous scaffolds through solvent evaporation from Pickering HIPEs. FTIR tests of scaffold $H_5P_5$-80 before and after loading of IBU were performed, and the results were displayed in Fig. S5. As observed, after loading of IBU, the peak at 1724 $cm^{-1}$ became stronger, which should be due to the combination and overlap of the stretching vibration peaks of -COOH groups from IBU at 1721 $cm^{-1}$ [53] and -C=O groups from porous scaffold at 1724 $cm^{-1}$.[54] The FTIR result qualitatively verified the successful loading of IBU in porous scaffold. Furthermore, the inner pore structure of IBU-loaded scaffold $H_5P_5$-80 was observed using SEM. As can be seen, the inner pore structure of IBU-loaded scaffold (see Fig. S6) was not significantly changed compared with unloaded porous scaffold (Fig. 3b), suggesting that the addition of IBU into porous scaffolds was little influence on the inner pore structure. For efficient drug action, the drug loading efficiency is a critical index in the preparation of drug-loaded scaffolds. In this study, the IBU loading efficiencies of drug-loaded scaffolds prepared with 2.5, 5, 7.5, and 10 w/v% of g-HAp nanoparticle contents were 97.7 ± 1.8%, 98.2 ± 2.2%, 98.6 ± 2.6%, 99.1 ± 1.7%, respectively. The loading efficiencies of IBU in the porous scaffolds were actually higher than 97%, indicating that in situ solvent evaporation based on Pickering HIPE templates was an easy and effective approach to prepare the drug-loaded porous scaffolds.

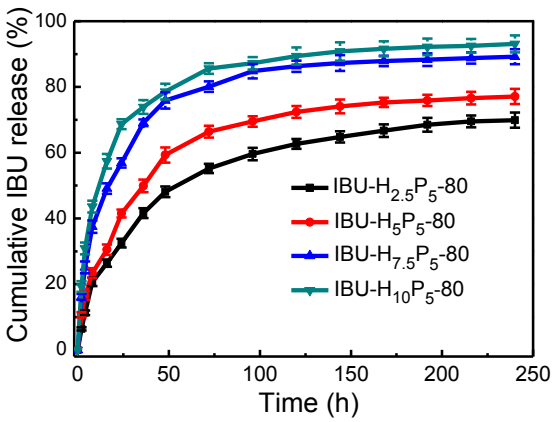


**Fig. 6.** In vitro release curves of IBU from different IBU-loaded porous scaffolds in PBS as a function of incubation time.

The release behavior of IBU from porous scaffolds was next investigated in vitro. **Fig. 6** presents the release curves of IBU in PBS buffer (pH 7.4) from porous scaffolds with various g-HAp nanoparticle concentrations. It was clear that all porous scaffolds showed similar drug release behaviors over the study period, which followed a biphasic pattern characterized by an initial fast release and subsequently a successive sustained release. For example, about 59.3% of IBU was released within the first 48 h, and around 77.1% IBU was released within 240 h from IBU-loaded scaffold $H_5P_5$-80. The initial fast release of all drug-loaded scaffolds could be ascribed to the rapid IBU release from outer surfaces and pore entrances. And in the later release phase, the successive sustained release might be due to the enhancement of drug diffusion path length and the interaction between the hydroxyl groups from the g-HAp nanoparticle surfaces and the carboxyl groups of IBU. Furthermore, it was also seen that the IBU release was obviously speeded up when the porous scaffold was fabricated at higher g-HAp nanoparticle concentration. This result might be mainly due to the fact that the addition of g-HAp nanoparticles into PCL matrix increased the hydrophilicity of porous scaffolds, which assisted in penetrating the release medium into the porous scaffolds, accelerated the dissolving and diffusing process of IBU in the release medium, and in turn resulted in a fast release of IBU. As the control group, the release behavior of free IBU was also determined at 37 °C in PBS buffer. As can be seen in Fig. S7, the release rate of free IBU was clearly fast, and larger than 90 % IBU was released within 60 min. In short, the above results showed that the IBU release from drug-loaded scaffolds was dependent on the g-HAp nanoparticle concentration of porous scaffolds. And the prepared porous scaffolds were able to provide controllable and sustained drug release, which could be usefull for the implant osseointegration.

**In vitro biocompatibility assessment**

In vitro cell culture experiments were performed to evaluate the biocompatibility of prepared porous scaffolds. BMSCs were cultured in vitro on the NC porous scaffolds with various g-HAp nanoparticle concentrations and on a commercially available tissue culture plates (TCPS) as a positive control. The cell viability of BMSCs on porous scaffolds and TCPS was evaluated using an MTT assay after 1 day, 4 days and 7 days culture. **Fig. 7**a shows the viability of BMSCs on porous scaffolds and TCPS, which demonstrates that BMSCs can adhere and proliferate on all porous scaffolds. As observed, viable BMSCs on all scaffolds significantly proliferated over the cultivation time. And the BMSCs cultured on the porous scaffolds prepared with relatively high g-HAp nanoparticle content showed a faster rate of cell proliferation, which indicated that the incorporation of g-HAp into PCL greatly facilitated attached cells to proliferate, and in turn suggested a high affinity of BMSCs for g-HAp nanoparticles. The above result might be connected with both the chemical composition and surface topography of the porous scaffolds. Incorporation of g-HAp nanoparticles into PCL matrix resulted in changing the chemical composition of the porous scaffolds, and the amount of HAp increased because the main composite in g-HAp nanoparticles was HAp. The addition of HAp into scaffolds was beneficial for the adsorption of several essential cell adhesion proteins (such asbronectin and vitronectin) during the cultivation process,[26] which

facilitated cell attachment and further accelerated cell proliferation. As shown in Fig. 1, the pore wall surfaces of NC porous scaffolds became rougher with increasing g-HAp nanoparticle content. This increased surface roughness of pore wall was also contributed to the increase of cell attachment and proliferation.[55] In addition, the OD values of both scaffold $H_{7.5}P_5$-80 and scaffold $H_{10}P_5$-80 were higher than that of the control sample (TCPS) after 7 days of cell culture. This could be attributed to the bigger space for cell growth and proliferation in 3D porous scaffolds compared with TCPS. In short, the ability of porous scaffolds to support BMSCs attachment, growth and proliferation gave an obvious indication of their biocompatibility.

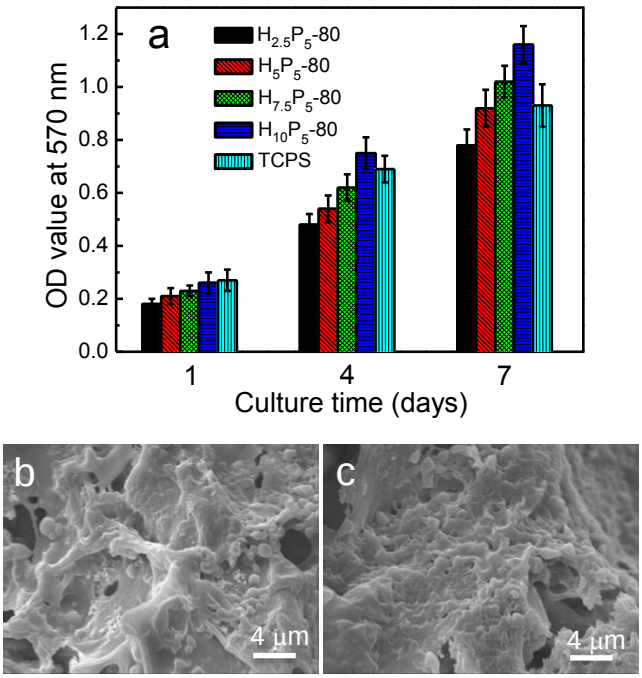


**Fig. 7** (a) Cell proliferation of BMSCs on porous scaffolds and TCPS as a function of incubation time, measured by MTT assay. (b, c) SEM images of BMSCs growth on scaffold $H_5P_5$-80 for different time periods: (b) 4 days, (c) 7 days.

The morphology of BMSCs was examined using SEM to further assess the biocompatibility of the porous scaffolds. Representative SEM images of BMSCs on scaffold $H_5P_5$-80 after 4 and 7 days of culture are shown in Fig. 7b,c. After 4 days of culture, the BMSCs had adhered well and spreaded on the pore wall surface of porous scaffold, and exhibited spindle-like elongated morphology with lamellipodium. More interestingly, after 7 days of culture, the BMSCs were completely spread on the pore wall surface of porous scaffold, and formed a confluent layer, implying the good cell viability of BMSCs on the porous scaffolds. Combined with the results from MTT assay and SEM observation, it is concluded that the porous scaffolds possessed good biocompatibility with BMSCs. Therefore, the developed bioactive g-HAp/PCL NC porous scaffolds were potentially useful in the field of bone tissue engineering.

## Conclusions

Highly porous g-HAp/PCL NC scaffolds with a well-defined interconnected and rough pore structure were facilely fabricated via solvent evaporation of templating g-HAp nanoparticle-stabilized Pickering HIPE droplets. The pore structure of fabricated scaffolds could be adjusted readily by altering g-HAp nanoparticle concentration, PCL concentration and internal phase volume fraction. The compression test results of porous scaffolds demonstrated that increasing g-HAp nanoparticle concentration enhanced the compressive modulus and stress. And in vitro biomineralization experiments exhibited that the apatite particles could be formed on the porous scaffolds, and higher g-HAp nanoparticle content added into PCL matrix promoted the formation of apatite particles. Furthermore, the anti-inflammatory drug IBU used as the model drug was added into oil phase to prepare IBU-loaded porous scaffolds. The in vitro drug release studies indicated that the loaded IBU displayed a sustained release property, which was important for biomedical applications to maintain long-term anti-inflammatory efficacy. And the IBU release rate from porous scaffolds enhanced with the increase in g-HAp nanoparticle concentration. In addition, in vitro cell culture assays demonstrated that BMSCs could adhere, spread, and proliferate on the porous scaffolds, showing the biocompatibility of porous scaffolds. Overall, all these results indicated that the fabricated NC porous scaffolds were potentially suitable biomaterials for bone tissue engineering. Besides, the solvent evaporation basing on templating Pickering HIPE droplets was a facile and effective way to produce biocompatible, bioactive and biodegradable porous scaffolds for bone tissue engineering application.

## Acknowledgements

This work was supported by the National Natural Science Foundation of China (21274046 and 21474032), the National Natural Basic Research Program of China (973 Program, 2012CB821500) and the Natural Science Foundation of Guangdong Province (S20120011057).

## Notes and references

[a]Research Institute of Materials Science, South China University of Technology, Guangzhou 510640, China. Fax & Tel: +86-20-2223-6269; E-mail: zhywang@scut.edu.cn.
[b]Guangdong Province Key Laboratory of Biomedical Engineering, South China University of Technology, Guangzhou, 510006, China.

† Footnotes should appear here. These might include comments relevant to but not central to the matter under discussion, limited experimental and spectral data, and crystallographic data.

Electronic Supplementary Information (ESI) available: Characterization of Pickering HIPEs and porous scaffolds. See DOI: 10.1039/b000000x/

1 M. Dash, S. K. Samal, C. Bartoli, A. Morelli, P. F. Smet, P. Dubruel and F. Chiellini, *ACS Appl. Mater. Interfaces*, 2014, **6**, 3211.
2 S. Z. Fu, P. Y. Ni, B. Y. Wang, B. Y. Chu, L. Zheng, F. Luo, J. C. Luo and Z. Y. Qian, *Biomaterials*, 2012, **33**, 4801.
3 Q. W. Zhang, V. N. Mochalin, I. Neitzel, K. Hazeli, J. J. Niu, A. Kontsos, J. G. Zhou, P. I. Lelkes and Y. Gogotsi, *Biomaterials*, 2012, **33**, 5067.

4 P. Wang, L. Zhao, J. Liu, M. D. Weir, X. D. Zhou and H. H. K. Xu, *Bone Res.*, 2014, **2**, 14017.
5 P. B. Zhang, Z. K. Hong, T. Yu, X. S. Chen and X. B. Jing, *Biomaterials*, 2009, **30**, 58.
6 M. Peter, N. Ganesh, N. Selvamurugan, S. V. Nair, T. Furuike, H. Tamura and R. Jayakumar, *Carbohydr. Polym.*, 2010, **80**, 687.
7 M. Cicuéndez, M. Malmsten, J. C. Doadrio, M. T. Portolés, I. Izquierdo-Barba and M. Vallet-Reg í, *J. Mater. Chem. B*, 2014, **2**, 49.
8 M. Angarano, S. Schulz, M. Fabritius, R. Vogt, T. Steinberg, P. Tomakidi, C. Friedrich and R. Mülhaupt, *Adv. Funct. Mater.* 2013, **23**, 3277.
9 H. J. Lee,Y. B. Kim , S. H. Kim and G. H. Kim, *J. Mater. Chem. B*, 2014, **2**, 5785.
10 S. Roohani-Esfahani, S. Nouri-Khorasani, Z. F. Lu, R. Appleyard and H. Zreiqat, *Biomaterials*, 2010, **31**, 5498.
11 C. L. He, X. B. Jin and P. X. Ma, *Acta Biomater.*, 2014, **10**, 419.
12 S. Z. Fu, P. Y. Ni, B. Y. Wang, B. Y. Chu, J. R. Peng, L. Zheng, X. Zhao, F. Luo, Y. Q. Wei and Z. Y. Qian, *Biomaterials*, 2012, **33**, 8363.
13 M. X. Liu, C. C. Wu, Y. P. Jiao, S. Xiong and C. R. Zhou, *J. Mater. Chem. B*, 2013, **1**, 2078.
14 C. M. Hu, S. Liu, Y. Zhang, B. Li, H. L. Yang, C. Y. Fan and W. G. Cui, *Acta Biomater.*, 2013, **9**, 7381.
15 J. Henkel, M. A. Woodruff, D. R. Epari, R. Steck, V. Glatt, I. C. Dickinson, P. F. M. Choong, M. A. Schuetz and D. W. Hutmacher, *Bone Res.*, 2013, **3**, 216.
16 J. P. Chen and Y. S. Chang, *Colloids Surf., B,* 2011, **86**, 169.
17 F. Peng, X. H. Yu and M. Wei, *Acta Biomater.*, 2011, **7**, 2585.
18 Y. Hu, S. W. Zou, W. K. Chen, Z. Tong and C. Y. Wang, *Colloids Surf., B*, 2014, **122**, 559.
19 H. Jiang, Y. Zuo, Q. Zou, H. N. Wang, J. J. Du, Y. B. Li and X. C. Yang, *ACS Appl. Mater. Interfaces*, 2013, **5**, 12036.
20 J. Yang, T. Long, N. F. He, Y. P. Guo, Z. A. Zhu and Q. F. Ke, *J. Mater. Chem. B*, 2014, **2**, 6611.
21 S. Z. Fu, X. H. Wang, G. Guo, S. Shi, M. Fan, H. Liang, F. Luo and Z. Y. Qian, *J. Biomed. Mater. Res. B*, 2011, **97**, 74.
22 A. Salerno, S. Zeppetelli, E. D. Maio, S. Iannace and P. A. Netti, *Macromol. Rapid Commun.*, 2011, **32**, 1150.
23 D. W. Zhang, O. J. George, K. M. Petersen, A. C. Jimenez-Vergara, M. S. Hahn and M. A. Grunlan, *Acta Biomater.*, 2014, **10**, 4597.
24 T. Q. Bao, R. A. Franco and B. T. Lee, *Biochem. Eng. J.*, 2012, **64**, 76.
25 J. J. Xue, M. He, Y. Z. Liang, A. Crawford, P. Coates, D. F. Chen, R. Shi and L. Q. Zhang, *J. Mater. Chem. B*, 2014, **2**, 6867.
26 J. Lee and H. S. Yun, *J. Mater. Chem. B*, 2014, **2**, 1255.
27 S. Z. Zhou, A. Bismarck and J. H. G. Steinke, *J. Mater. Chem.*, 2012, **22**, 18824.
28 Y. Hu, Y. Yang, Y. Ning, C. Y. Wang and Z. Tong, *Colloids Surf., B*, 2013, **112**, 96.
29 S. Eshraghi and S. Das, *Acta Biomater.*, 2012, **8**, 3138.
30 Y. Wang, J. Dai, Q. C. Zhang, Y. Xiao and M. D. Lang, *Appl. Surf. Sci.*, 2010, **256**, 6107.
31 H. J. Lee, H. W. Choi, K. J. Kim and S. C. Lee, *Chem. Mater.*, 2006, **18**, 5111.
32 R. M. Boehler, S. Shin, A. G. Fast, R. M. Gower and L. D. Shea, *Biomaterials*, 2013, **34**, 5431.
33 J. A. Sowjanya, J. Singh, T. Mohita, S. Sarvanan, A. Moorthi, N. Srinivasan and N. Selvamurugan, *Colloids Surf., B*, 2013, **109**, 294.
34 W. J. Lu, J. S. Sun and X. Y. Jiang, *J. Mater. Chem. B*, 2014, **2**, 2369.
35 A. V ázquez, C. Rodr íguez-Abreu, J. Esquena, A. Menner and A. Bismarck, *Langmuir*, 2011, **27**, 13342.
36 S. W. Zou, Z. J. Wei, Y. Hu, Y. H. Deng, Z. Tong and C. Y. Wang, *Polym. Chem.*, 2014, **5**, 4227.
37 Z. Zheng, X. H. Zheng, H. T. Wang and Q. G. Du, *ACS Appl. Mater. Interfaces*, 2013, **5**, 7974.
38 P. J. Colver and S. A. F. Bon, *Chem. Mater.*, 2007, **19**, 1537.
39 Z. F. Li, M. D. Xiao, J. F. Wang and T. Ngai, *Macromol. Rapid Commun.*, 2013, **34**, 169.
40 Y. H. Chen, N. Ballard and S. A. F. Bon, *Chem. Commun.*, 2013, **49**, 1524.
41 D. Y. Zang and P. S. Clegg, *Soft Matter*, 2013, **9**, 7042.
42 X. D. Li, G. Q. Sun, Y. C. Li, J. C. Yu, J. Wu, G. H. Ma and To Ngai, *Langmuir*, 2014, **30**, 2676.
43 Y. Hu, X. Y. Gu, W. K. Chen, S. W. Zou and C. Y. Wang, *Macromol. Mater. Eng.*, 2014, **299**, 1070.
44 M. S. Silverstein, *Prog. Polym. Sci.*, 2014, **39**, 199.
45 Z. F. Li, T. Ming, J. F. Wang and T. Ngai, *Angew. Chem. Int. Ed.*, 2009, **48**, 8490.
46 T. S. Skelhon, N. Grossiord, A. R. Morgan and S. A. F. Bon, *J. Mater. Chem.*, 2012, **22**, 19289.
47 Y. Zhang, X. H. Zheng, H. T. Wang and Q. G. Du, *J. Mater. Chem. A*, 2014, **2**, 5304.
48 F. Qi, J. Wu, G. Q. Sun, F. F. Nan, T. Ngai and G. H. Ma, *J. Mater. Chem. B*, 2014, **2**, 7605.
49 Y. L. Zhao, G. N. Yin, Z. Zheng, H. T. Wang and Q. G. Du, *J. Polym. Sci. Part A: Polym. Chem.*, 2011, **49**, 5257.
50 Y. Yang, Z. J. Wei, C. Y. Wang and Z. Tong, *Chem. Commun.*, 2013, **49**, 7144.
51 F. F. Nan, J. Wu, F. Qi, Q. Z. Fan, G. H. Ma and T. Ngai, *J. Mater. Chem. B*, 2014, **2**, 7403.
52 Y. Hu, X. Y. Gu, Y. Yang, J. Huang, M. Hu, W. K. Chen, Z. Tong, and C. Y. Wang, *ACS Appl. Mater. Interfaces*, 2014, **6**, 17166.
53 Z. J. Ma, H. J. Ji, Y. Teng, G. P. Dong, D. Z. Tan, M. J. Guan, J. J. Zhou, J. H. Xie, J. R. Qiu and M. Zhang, *J. Mater. Chem.*, 2011, **21**, 9595.
54 E. J. Lee, S. H. Teng, T. S. Jang, P. Wang, S. W. Yook, H. E Kim and Y. H. Koh, *Acta Biomater.*, 2010, **6**, 3557.
55 D. L. Cheng, X. D. Cao, H. C. Gao and Y. J. Wang, *J. Mater. Chem. B*, 2013, **1**, 3322.

# A table of contents entry

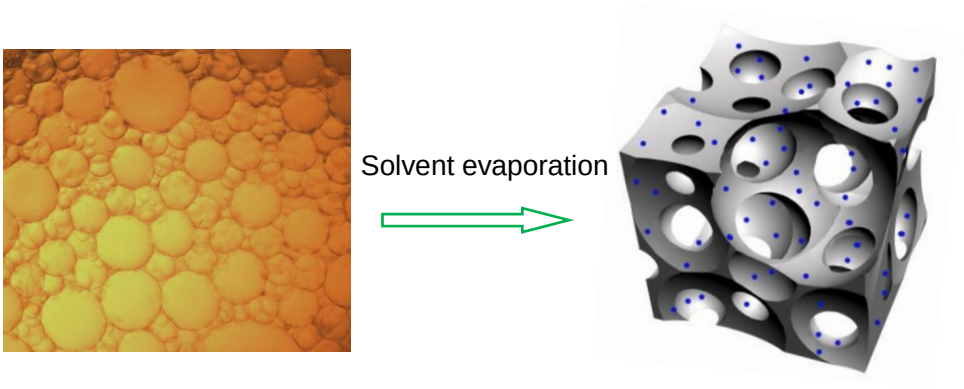


Hydroxyapatite/polycaprolactone nanocomposite scaffolds were facilely fabricated by solvent evaporation based on water-in-dichloromethane Pickering high internal phase emulsions.